JOURNAL OF AIRCRAFT
Vol. 41, No. 4, July–August 2004

Computational-Fluid-Dynamics-Based Enhanced Indicial Aerodynamic Models

Jayanarayanan Sitaraman* and James D. Baeder†
University of Maryland, College Park, Maryland 20742

Direct Euler calculations were performed to verify the accuracy of linearized airload models and to generate a numerical database for the determination of generalized sharp-edged vertical gust response functions. The field velocity approach was used in the computational fluid dynamics (CFD) code to incorporate the impulsive boundary conditions that were characteristic of the problems studied. Linearized airload models were constructed in three dimensions by coupling the indicial models obtained in two dimensions with a Weissinger-L vortex panel method. The vortex panel method was suitably modified to include the shed near wake effects and impulsive boundary conditions. Studies conducted on step change in angle of attack and step change in pitch rate for a finite wing showed that the linearized models are sufficiently accurate in predicting the sectionwise air loads. Generalized gust functions were determined with a constrained minimization of least-square error with a CFD-generated database. Studies on airfoil vortex interaction and parallel blade vortex interaction showed excellent correlation of results from linearized aerodynamic model with the corresponding CFD calculations for both lift and pitching moment response. Overall, the linearized methods were found to produce sufficiently accurate results compared to CFD calculations, taking about four orders of magnitude less computational time.

Nomenclature

A_i, b_i	=	indicial coefficients
a	=	speed of sound in undisturbed medium
C_l	=	lift coefficient
C_{l_α}	=	lift curve slope, $(2\pi/\beta)$
C_m	=	moment coefficient
C_{m_α}	=	pitching moment curve slope
c	=	chord length of the airfoil
M	=	Mach number
R	=	radius
r_c	=	vortex core radius
s	=	nondimensional time
t	=	time
U_∞	=	freestream velocity
u, v, w	=	aerodynamic velocity field
u', v', w'	=	perturbation velocity field
V_g	=	gust convection velocity
w_g	=	gust magnitude
X_c	=	horizontal separation between blade and vortex
Z_c	=	vertical separation between blade and vortex
α	=	angle of attack
β	=	Prandtl–Gleurt correction factor, $[\sqrt{(1-M^2)}]$
Γ	=	vortex strength
Λ	=	sweep
λ	=	speed ratio
μ	=	advance ratio
$\Psi(s)$	=	generalized gust function
ψ	=	azimuth
Ω	=	angular velocity

Presented as Paper 2000-2465 at the AIAA Fluids 2000 Symposium, Denver, CO, 19–22 June 2000; received 25 June 2002; revision received 1 May 2003; accepted for publication 25 August 2003.

*Graduate Research Assistant, Department of Aerospace Engineering.
†Associate Professor, Department of Aerospace Engineering. Associate Fellow AIAA.

Introduction

COMPUTATIONAL fluid dynamics (CFD) techniques, when used for modeling unsteady aerodynamic phenomena, require a large amount of computational resources and, hence, are impractical from a designer's point of view. Hence, most comprehensive design codes use linearized aerodynamic models for the practical computation of unsteady aerodynamics. These linearized models make use of a functional representation for the indicial aerodynamic lift and pitching moment responses in terms of blade motion and gust functions.[1] Three-dimensional effects are included with a suitable method, for example, either lifting line or lifting surface methods. However, the accuracy of these linearized methods was always a concern. Therefore, validation of the results obtained from the linearized methods with those from direct CFD calulations is required, as is an understanding of their limitations.

The so-called indicial response functions, which describe the aerodyanamic load responses to step changes in boundary conditions, constitute the core of a linearized unsteady aerodynamic model. The indicial response functions used in present day comprehensive codes are limited in their generality and, hence, are not completely effective for modeling the complete unsteady flow regime in which a rotor blade operates. The operating Mach number for a particular section of the rotor blade depends on its radial position. Therefore, the indicial response functions need to be generalized with the Mach number. Another important parameter while the problem of the interaction of the rotor blade with the shed tip vortices is studied the relative speed of the vortices with respect to the blade. The gust speed ratio can be defined as

$$\lambda = V/(V + V_g) \tag{1}$$

where V is the velocity of the blade element and V_g is the component of the gust convection velocity in the direction of V. Therefore, the denominator in the Eq. (1), $V + V_g$, represents the velocity of the vortex with respect to the blade. The parameter λ can, therefore, be used for generalizing the indicial response functions for interactions with convecting tip vortices. The assumption made in most rotor aerodynamic analyses is that the tip vortices (and corresponding induced velocity field) are stationary with respect to the rotor, that is, $\lambda = 1$. However, the self-induced velocities from the trailed vortex wake system result in continuously changing and nonuniform convection of the tip vortices with respect to the rotor. This can produce values of λ that can be less than or greater than unity.

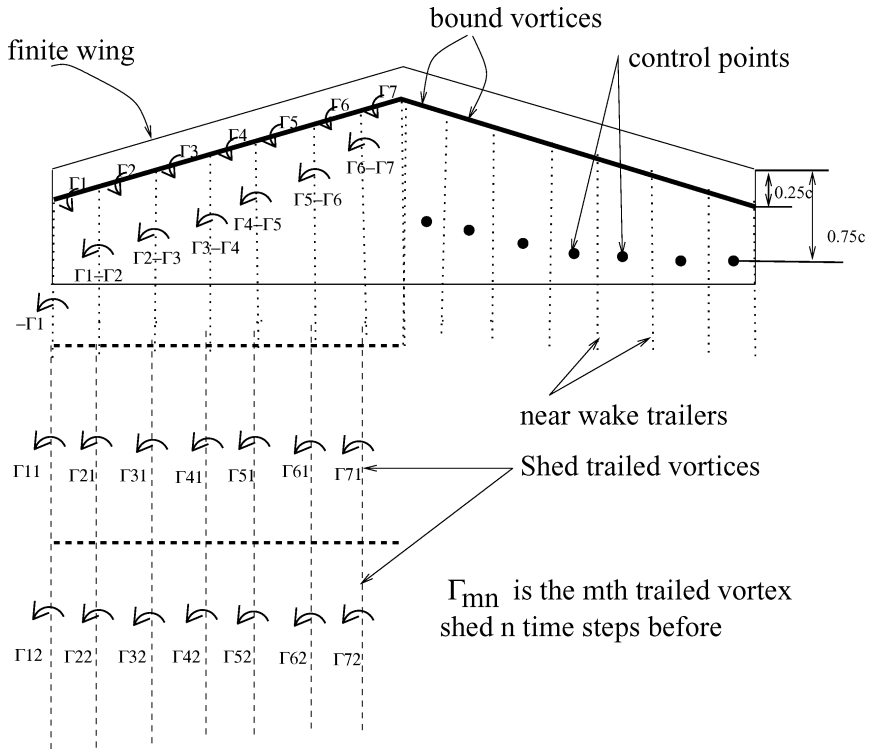

Fig. 1 Weissinger-L unsteady model.

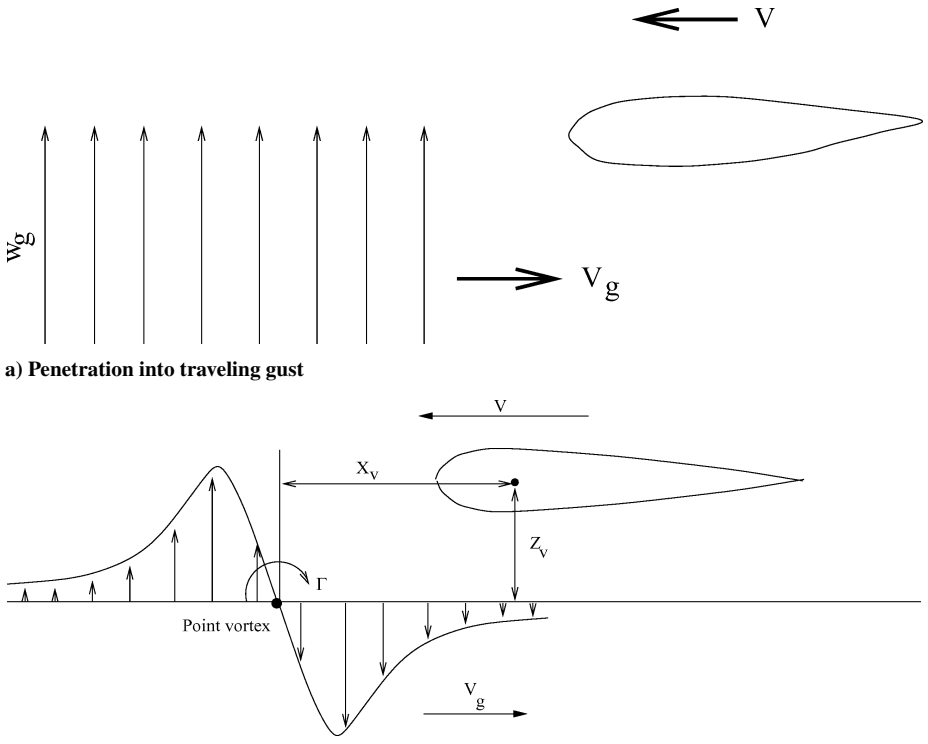

Fig. 2 Airfoil interaction schematics.

Although exact analytical results exist for the incompressible flow case, indicial responses in subsonic compressible flow are known analytically for only a short period of time. The work by Bisplinghoff et al.[2] provides the basis for the development of indicial aerodynamic models for compressible flows. Lomax et al.[3] and Lomax[4] obtained the exact analytical results that are valid for a short period of time for indicial responses caused by step changes in angle of attack, pitch rate, and for penetration of a sharp-edged gust in subsonic compressible flow. Mazelsky[5] determined the reciprocal equations relating the lift and moment acting on an airfoil undergoing harmonic oscillations in compressible flow to the indicial lift and moment functions for a pitching airfoil. This analysis indicated the necessity of two indicial functions to describe the airloads on an oscillating airfoil completely, one for describing the effects caused by the angular position and the other representing the effect caused by varying pitch velocity. Miles[6] was

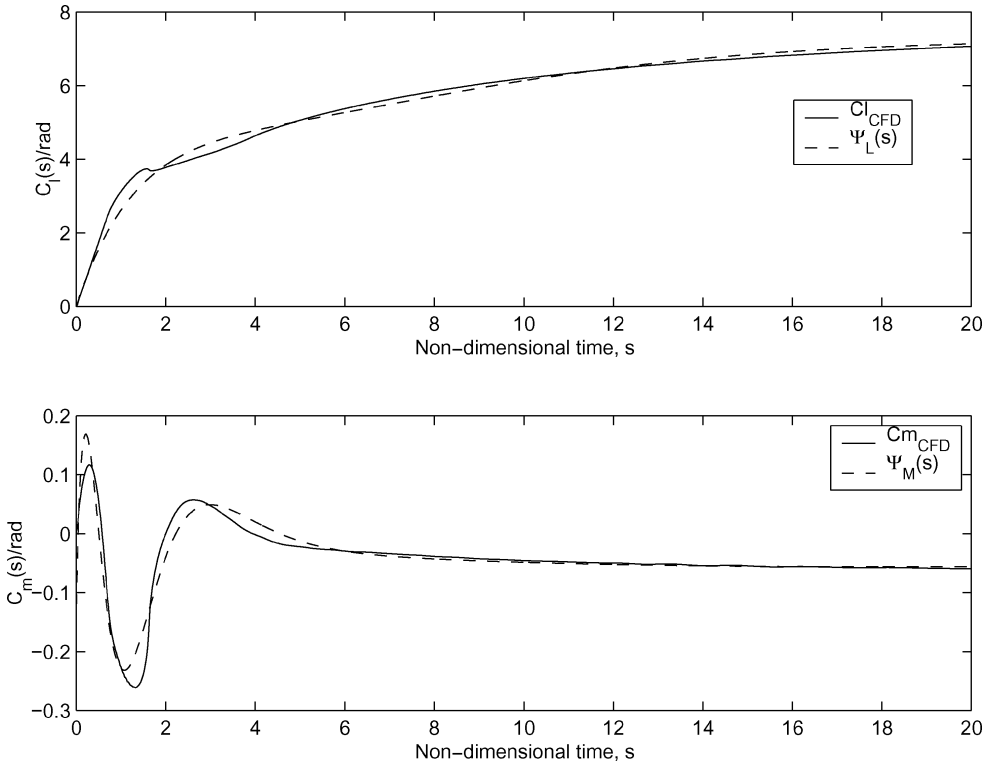

Fig. 3 Lift and pitching moment response and approximate gust functions for $(M, \lambda) = (0.5, 0.8)$.

the first to study the unsteady load responses when encountering traveling vertical sharp-edged gusts for a thin airfoil in incompressible flow in terms of the gust speed ratio λ. Miles[6] also showed that, as the propagation speed of the traveling gust is increased from zero to ∞, the solution for the lift changes from the Küssner result to the Wagner result. Drischler and diedrich[7] extended the approach followed by Mazelsky and Drischler[8] to calculate semi-analytical approximations for the indicial lift and moment response to penetration of a sharp-edged traveling vertical gust for wings in incompressible and supersonic two-dimensional flow. Leishman[1] developed generalized approximations to the indicial lift response because of angle of attack and pitch rate in two-dimensional subsonic flow using experimental data and exact analytical results. This approach extracted intermediate forms of indicial lift response, generalized in terms of Mach number and pitch axis locations. A reverse flow theorem based approach was used by Leishman[9] for studying unsteady airload responses while an airfoil encounters traveling gusts or vortices. Singh[10] determined the exact analytical solution for lift and pitching moment response when a traveling vertical gust is encountered by use of an airfoil in subsonic compressible flow using Evvard's[11] theorem. Singh[10] also developed generalized approximations to lift response using a CFD-generated database and used them to study the problem of airfoil–vortex interaction (AVI).

The precursors to this work are those by Singh and Baeder[12] on the direct calculation of the indicial lift response for a finite wing and on the development of generalized gust functions for lift responses to traveling gusts.[13]

The objective of the present study is twofold. First, the accuracy of the linearized methods compared to the direct Euler computations is investigated with CFD, and some improvements are proposed to the functional representations for indicial response. The second objective is to develop generalized indicial gust functions for representing both the lift and pitching moment responses for an airfoil penetrating through a sharp-edged moving gust with use of the numerical database obtained from direct CFD computations. Such a generalized gust function would allow the use of superposition to find the total response caused by any arbitrary shaped moving gust.

Methodology

Computations Using CFD

Governing Equations

Because the quantities of interest in this study are the responses of the lift and moment coefficients to unsteady aerodynamic phenomena, the Euler equations are chosen as the governing equations for computation. The Euler equations are chosen because they are able capture nonlinearities in the flowfield caused by transonic effects more accurately than the potential equations, while remaining computationally less intensive than the Navier–Stokes equations. Also, while the Euler equations are being solved, it is not necessary to explicitly impose an unsteady Kutta condition for the vorticity in the wake region. The linear and nonlinear effects of compressibility are more prominent than the effects of viscosity on the aerodynamic quantities of interest. Hence, the use of inviscid computations for this study is justifiable.

Algorithm

The Euler computations are performed with the TURNS[14,15] research code, which has been applied to a variety of helicopter problems. The TURNS code uses Roe's upwinding with higher-order MUSCL-type limiting on the right-hand side for spatial accuracy. The left-hand side is processed with a lower-upper symmetric Gauss–Seidel implicit operator to increase stability and robustness. Unfortunately, the use of a spectral radius approximation in the implicit scheme renders the method only first-order accurate in time. Therefore, in this study, a second-order backward difference in time is used along with Newton-type subiterations to restore formal second-order time accuracy.

Incorporation of Indicial Boundary Conditions

The field velocity approach is used to incorporate the boundary conditions for simulating a step change in angle of attack, a step change in pitch rate, and the penetration of a finite wing/rotor blade into a sharp-edged moving gust. The effect of an impulsive change in boundary conditions is simulated by superposing a velocity field equivalent to the impulsive change over the freestream conditions. This superposed velocity field is modeled by modification of the

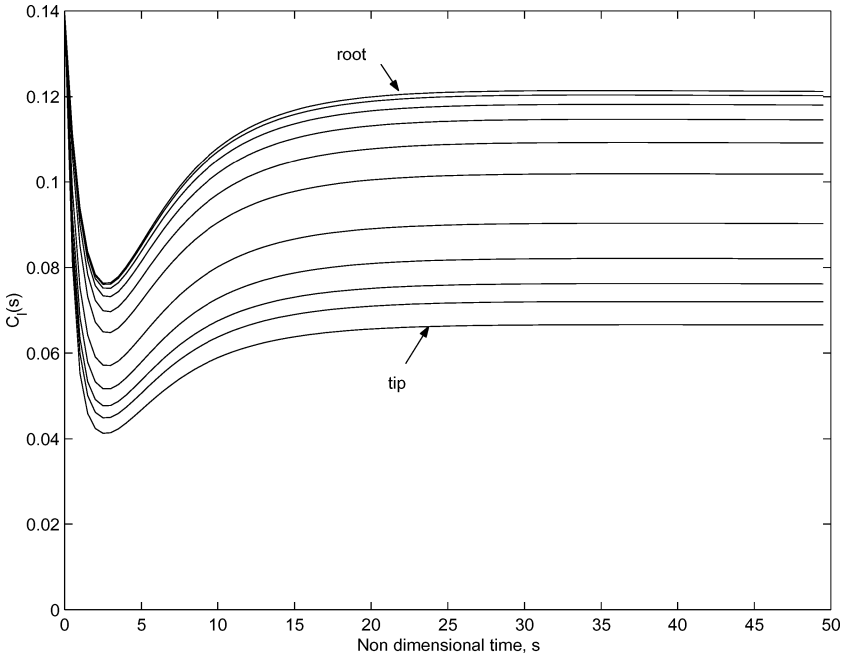

a) Linearized aerodynamics

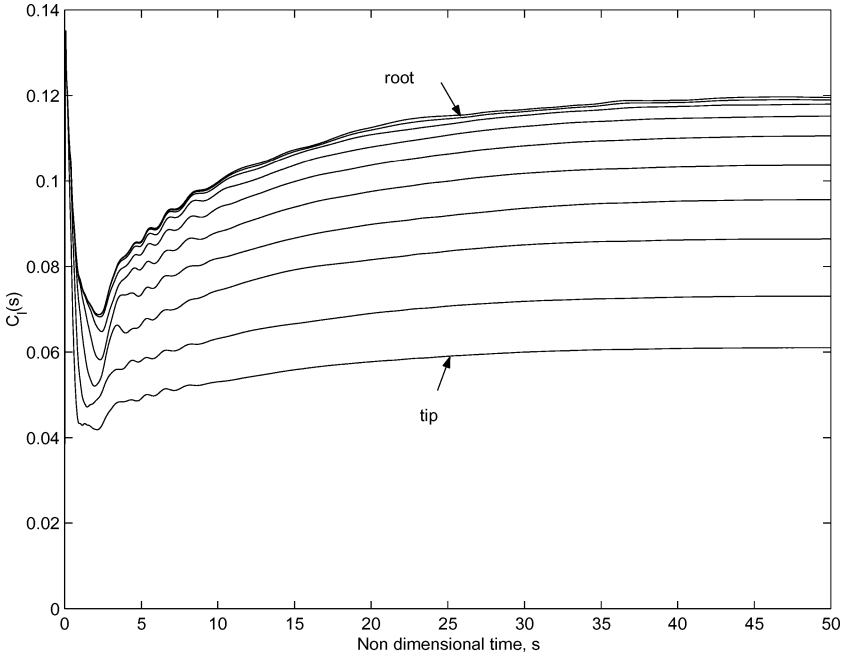

b) CFD

Fig. 4 Lift response for step change in angle of attack ($M = 0.5$, $\Delta\alpha = 1$ deg, $AR = 13.6$).

grid time metrics. There is no actual distortion or movement of the mesh, but this effect is obtained by modification of the grid time metrics suitably. Mathematically, the field velocity approach can be explained by considering the velocity field V in the computational domain. It can be written as

$$V = (u - x_\tau)i + (v - y_\tau)j + (w - z_\tau)k \tag{2}$$

where u, v, and w are components of the velocity along the coordinate directions and x_τ, y_τ, and z_τ are the grid time metrics components. For the flow over a stationary wing, these components are zero. Let an impulsive change in boundary condition be represented by a velocity field (u', v', w'). Thus, the velocity field becomes

$$V = (u - x_\tau + u')i + (v - y_\tau + v')j + (w - z_\tau + w')k \tag{3}$$

The field velocity approach models this changed velocity field by modifying the time metrics.

The modified time metrics are defined as

$$\tilde{x}_\tau i + \tilde{y}_\tau j + \tilde{z}_\tau k = (x_\tau - u')i + (y_\tau - v')j + (z_\tau - w')k \tag{4}$$

The fidelity of this approach in calculating responses to impulsive boundary conditions was validated by Singh and Baeder,[12] who compared numerical results for a two-dimensional airfoil with exact linear analytical results. This method is also being extended to simulate the interaction of rotor blades with their complicated wake structure.

Linearized Aerodynamic Model

The linearized aerodynamic model uses a Weissinger-L potential flow model to incorporate three-dimensional effects. The input for

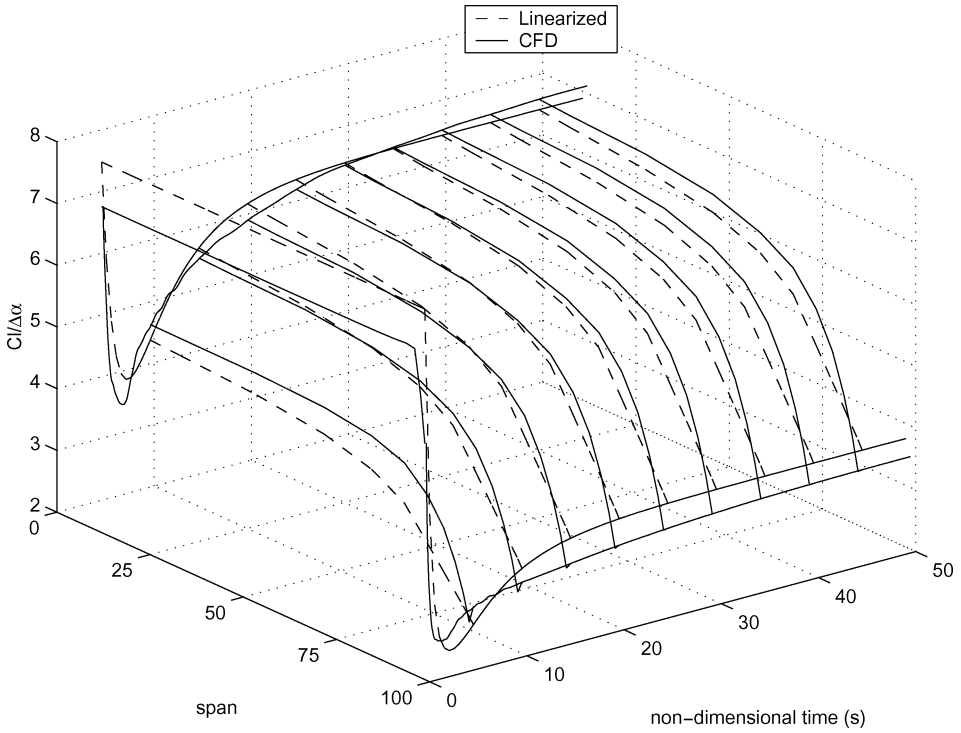

Fig. 5 Lift variation along span ($M = 0.5$).

the Weissinger-L model is obtained from the two-dimensional lift and pitching moment responses that are known from their approximate functional representations.

Weissinger-L Model

Weissinger theory or extended lifting line theory, differs from lifting line theory in several respects (see Ref. 16). It is really a simple panel method (a vortex lattice method with only one chordwise panel), rather than a corrected strip theory method as is lifting line theory. This model works for wings with sweep and converges to the correct solution in both the high and low aspect ratio limits. The basic concept is computation of the strengths of each of the bound vortices required to keep the flow tangent to the wing surface at a set of control points. Each horseshoe vortex consists of a bound vortex leg and two trailing vortices. This arrangement automatically satisfies the Helmholtz requirement that no vortex line ends in the flow. The trailing vortices extend to infinity behind the wing for a steady-state calculation; for an unsteady calculation, the trailing vortices are made to extend to a finite length equal to the distance traveled by the wing in the user-specified time-step value. The trailed vortices are assumed to be shed every time step, and, for the computation at any time, the effects of all of the vortices shed until that time are included on the right-hand side, as shown in Fig. 1. [Right-hand side (RHS) corresponds to the total effective gust at any control point.] Note that the effect of the shed bound vortices are not included explicitly because they are incorporated implicitly in the functional representation of the two-dimensional indicial response.

Formulation

The bound vortices are assumed to be located at the local quarter-chords, and the control points are chosen to be at three-quarter-chord, as shown in Fig. 1. If the horseshoe vortex at spanwise station j produces a downwash velocity involving the aerodynamic influence coefficient (AIC), of $\mathrm{AIC}_{ij}\Gamma_j$ at station i, then the linear system of equations representing the boundary condition of no normal flow at the surface at the control points is given by

$$[\mathrm{AIC}]\{\Gamma_i\} = U_\infty\{\alpha\} \tag{5}$$

Scully's[17] vortex model is assumed for all of the vortex filaments. A Biot–Savart integration is used to find the aerodynamic influence coefficients. This is the steady-state formulation of the Weissinger-L model. For an unsteady calculation, such as in an indicial change in boundary conditions, the circulation strength of the bound vortices vary with time. For such a case, the equations are modified as

$$[\mathrm{AIC}]\{\Gamma_i(t)\} = U_\infty\{\alpha(t)\} + \left\{V^i_{\mathrm{gust}}\right\} \tag{6}$$

where $\alpha(t) = Cl(t)/Cl_\alpha$, $Cl(t)$ is the unsteady two-dimensional indicial lift response, and V^i_{gust} is the downwash induced by all of the trailed vortices shed at the preceding time steps at the ith control point. The effects of taper and sweep are inherent from the geometry of the wing because the vortex filaments are placed at appropriate locations based on the geometric information. For wings with varying twist, the angle-of-attack component in the RHS is changed as $\theta_i + \alpha(t)$, where θ_i is the twist at the control point i. Effects of Mach number are inherent from the two-dimensional indicial model. For swept wings, the effective Mach number is taken as $M_\infty \cos(\Lambda)$, where Λ is the sweep angle.

Indicial Response Formulation

An indicial response to an impulsive boundary condition consists, in general, of two distinct regions, each having different flow physics, with an intermediate overlapping region. The initial part of the response is caused by the pistonlike motion of the wing, which causes a difference in pressure on the upper and lower surfaces. This initial loading is called the noncirculatory loading. The noncirculatory loading decays rapidly from the initial value within a few chord lengths of the distance traveled. This loading can be computed directly for two-dimensional subsonic and supersonic flow quite accurately with linear piston theory. For example, the initial value of the lift magnitude for a step change in angle of attack as given by linear piston theory is

$$C_L(T = 0) = (4/M)\Delta\alpha \tag{7}$$

where M is the freestream Mach number and $\Delta\alpha$ is the step change in angle of attack.

The second part of the response is related to the steady-state response to the effective change in boundary condition caused by

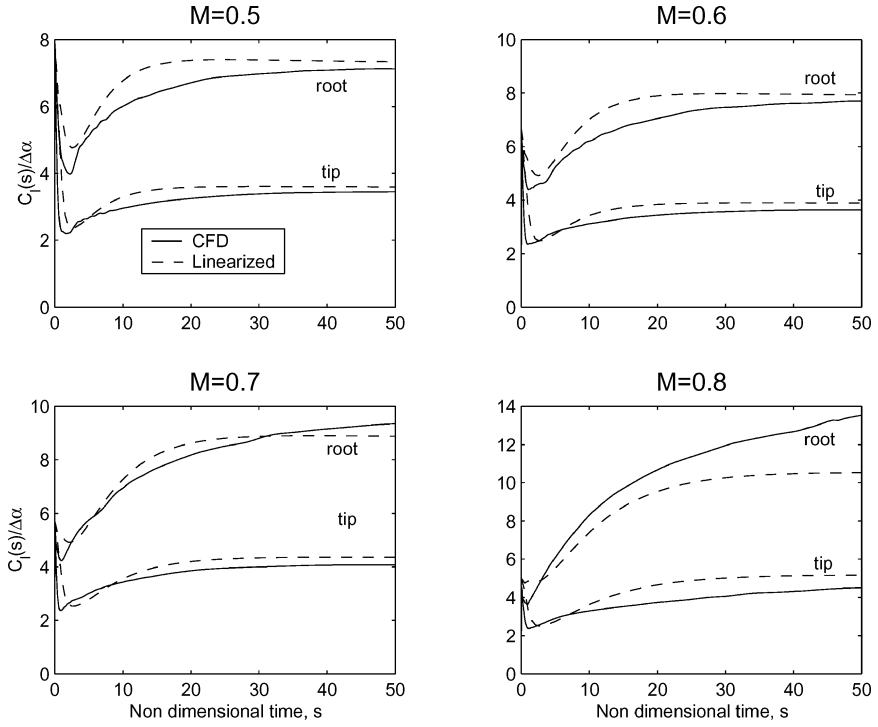

a) Lift response

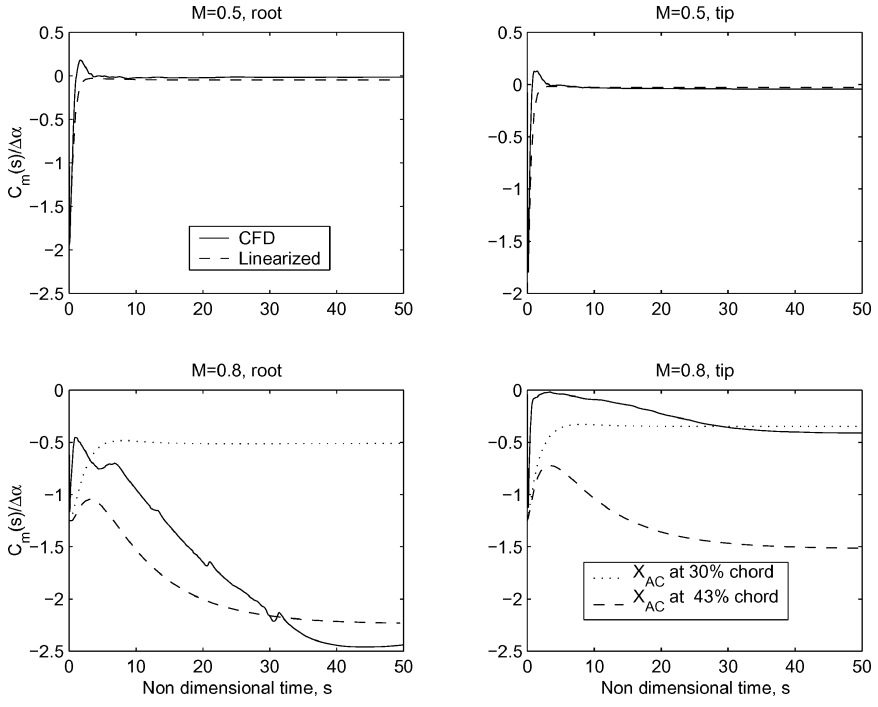

b) Pitching moment response

Fig. 6 Response from CFD and linearized models for step change in angle of attack at the root and tip of the wing, $M = 0.5$–0.8.

the impulsive input. This part is called the circulatory response; it is asymptotically reached after the perturbation caused by the step input and is a result of the change in bound circulation. This part can be accurately determined with quasi-steady theory. In the case of a step change in angle of attack, the final value of lift is given by quasi-steady theory as

$$C_L(T \to \infty) = \left(2\pi \Big/ \sqrt{1 - M^2}\right)\Delta\alpha \tag{8}$$

The main problem in the determination of the indicial response is the calculation of the response in the intermediate overlapping region. The flow is highly unsteady, and there are no closed-form solutions available for the development of the flow from the initial input to the steady state for compressible flow.

Generalized Indicial Gust Function

A generalized indicial gust function, as described earlier, represents the lift/pitching moment response to an airfoil penetrating through a traveling vertical gust (Fig. 2a). Such functions are necessary for rotorcraft problems because there is a variation in Mach number and gust speed ratio in both azimuth and span. The speed ratio λ follows the same definition as given by Eq. (1).

Functional Representation of Generalized Gust Function

Exponential terms are usually used in conventional gust functions because these facilitate the recursive evaluation of the Duhamel integral (see Ref. 18). The Duhamel integral, or superposition, is the method used to find the total response caused by an arbitrarily shaped gust in the time domain. However, the gust responses for the interaction of an airfoil with a traveling gust exhibits shapes that may not be curve fit satisfactorily with simple exponential functions alone. Singh[10] has developed algorithms for recursively evaluating the Duhamel integral using terms of the form $A_i s e^{-b_i s}$. These terms allow for the initial linear growth in time. In this study, a combination of such functions and exponential functions are chosen to represent the generalized gust functions. Investigations conducted favored the use of functions of the following form

$$\Psi_L(M, \lambda, s) = (Cl_\alpha w_g / V) \times \left(1 + A_1 s e^{-b_1 s} + A_2 e^{-b_2 s} + A_3 e^{-b_3 s} + A_4 e^{-b_4 s}\right) \tag{9}$$

for the lift response and

$$\Psi_M(M, \lambda, s) = (w_g / V) \times \left(A_1 s e^{-b_1 s} + A_2 s e^{-b_2 s} + A_3 s e^{-b_3 s} + A_4 s e^{-b_4 s}\right) \tag{10}$$

for the pitching moment response.

Typical shapes of the lift and pitching moment responses from CFD calculations and the generalized gust functions used to curve fit them are shown in Fig. 3. The dependence of the A_i and the b_i on Mach number and speed ratio are given in Table 1.

Determination of Indicial Coefficients

The database generated by direct Euler computations in two dimensions is used to determine the coefficients of the approximate functional representations to the unsteady response. The least-square error between the approximate functions and CFD-generated response is minimized with a commercial optimization package, DOT.[10] Constraints are imposed on the minimization to preserve

Table 1 Coefficients determined for the generalized indicial gust functions

Coefficient	Variation
	Lift response function
A_1	$0.4724 - 0.1842\lambda$
b_1	$0.6010 - 0.2059\lambda$
A_2	$1.0260 + 0.3959\beta$
b_2	$-0.2250 + 0.5645\beta$
A_3	1.6517
b_3	0.3518
A_4	$-1 - A_2 - A_3$
b_4	$\left(-\frac{\mathrm{d}Cl/\mathrm{d}s\|_{(s=0)}}{Cl_\alpha} + A_1 - A_2 b_2 - A_3 b_3\right) \Big/ A_4$
	Pitching moment response function
A_1	$-0.0176 + 0.00665\lambda$
b_1	$0.8751 - 3.2133M + 3.1448M^2$
A_2	$139.1916 - 123.8419\lambda$
b_2	$2.2994 - 1.5214M$
A_3	$212.0454 - 190.8123\lambda$
b_3	$2.2963 - 2.2459M$
A_4	$-347.2716 + 311.1876\lambda$
b_4	$2.5951 - 1.8481M$

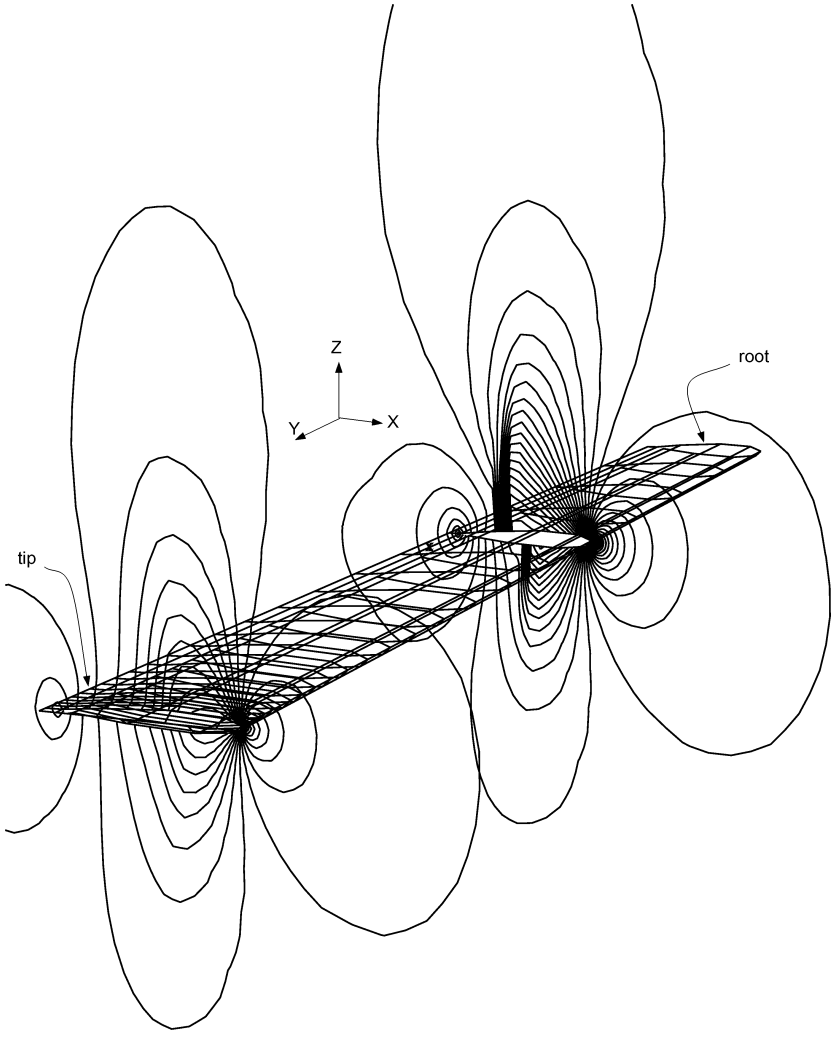

Fig. 7 Pressure contours at the root and tip of the finite wing at steady state, attained after a step change in angle of attack for a $M = 0.8$.

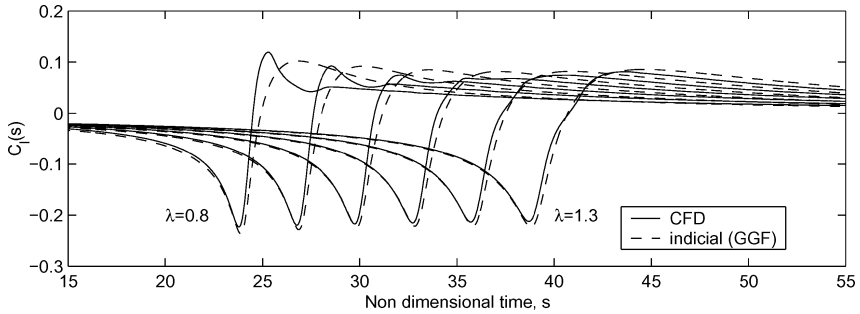

a) $M = 0.5$

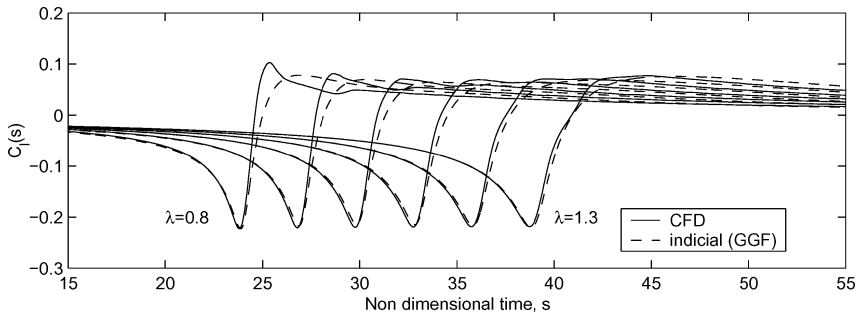

b) $M = 0.6$

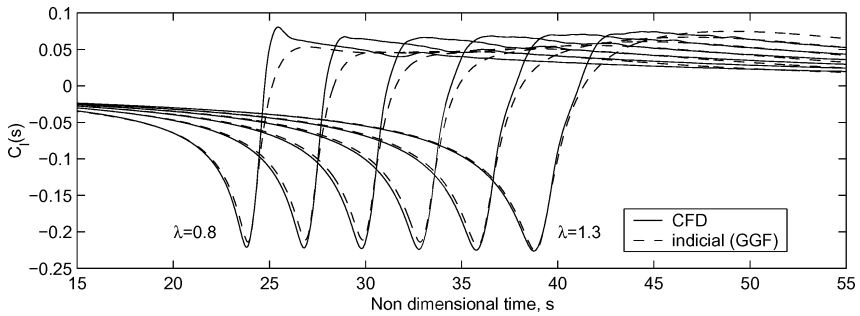

c) $M = 0.7$

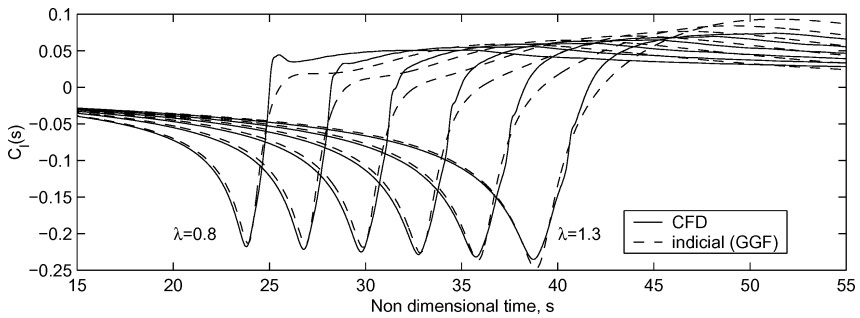

d) $M = 0.8$

Fig. 8 Lift response of AVI for $M = 0.5$, 0.6, 0.7, and 0.8 and $\lambda = 0.8$–1.3.

the analytical value of the initial slope and the final or steady-state value of the lift. The indicial coefficients are optimized over a range of Mach numbers and gust speed ratios to determine the generalized gust function. The objective functions for the optimization problem is formulated as

$$F_L = \sum_{j_m=1}^{N_m} \sum_{j_\lambda=1}^{N_\lambda} \sum_{j_s=1}^{N_s} \left[C_{l_{\text{CFD}}}(M, \lambda, s) - \Psi_L(M, \lambda, s) \right]^2 \quad (11)$$

$$F_M = \sum_{j_m=1}^{N_m} \sum_{j_\lambda=1}^{N_\lambda} \sum_{j_s=1}^{N_s} \left[C_{m_{\text{CFD}}}(M, \lambda, s) - \Psi_M(M, \lambda, s) \right]^2 \quad (12)$$

Where $C_{l_{\text{CFD}}}$ and $C_{m_{\text{CFD}}}$ are the lift and pitching moment response derived by the direct Euler computation for various Mach numbers and speed ratios. $\Psi_L(M, \lambda, s)$ and $\Psi_M(M, \lambda, s)$ are the approximate gust functions representing the indicial responses. The indices j_M, j_λ, and j_s represent the indices in Mach number, speed ratio, and nondimensional time. The whole equation signifies that the optimization is conducted to minimize the least-square error between the approximate functions and airload time histories for a range of Mach numbers and speed ratios. When the generalized gust functions (GGF) for lift response are determined, equality constraints that make the initial value zero and the initial slope match that obtained from the exact analytical results have to be adopted. These constraints are applied implicitly by determination of two of the coefficients in terms of the others, as seen in Table 1. A_4 and b_4 are the coefficients that are implicitly determined. The use of the condition $\Psi_L(M, \lambda, 0) = 0$ for a unit change in gust magnitude $w_g/V = 1$

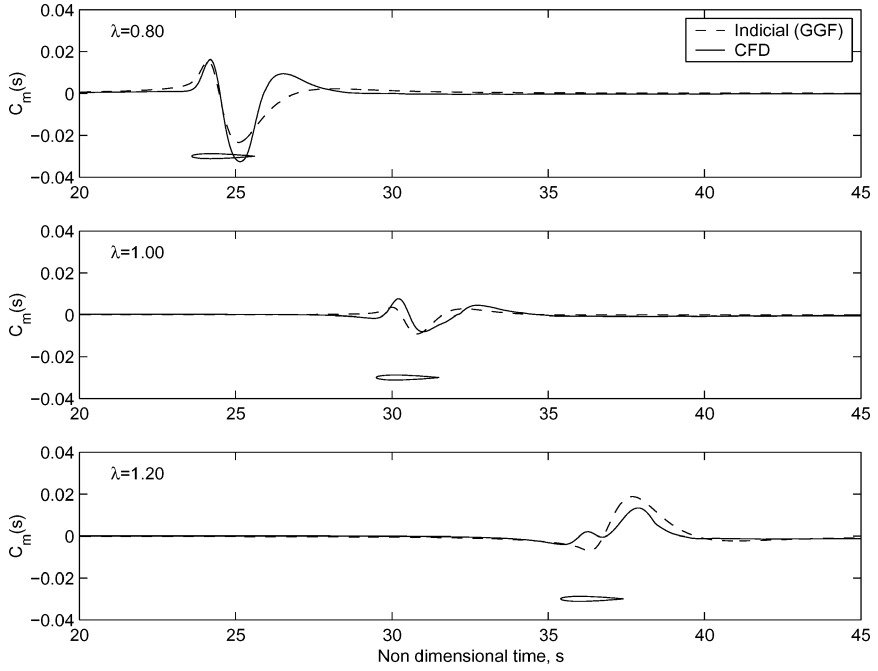

a) $M = 0.5$

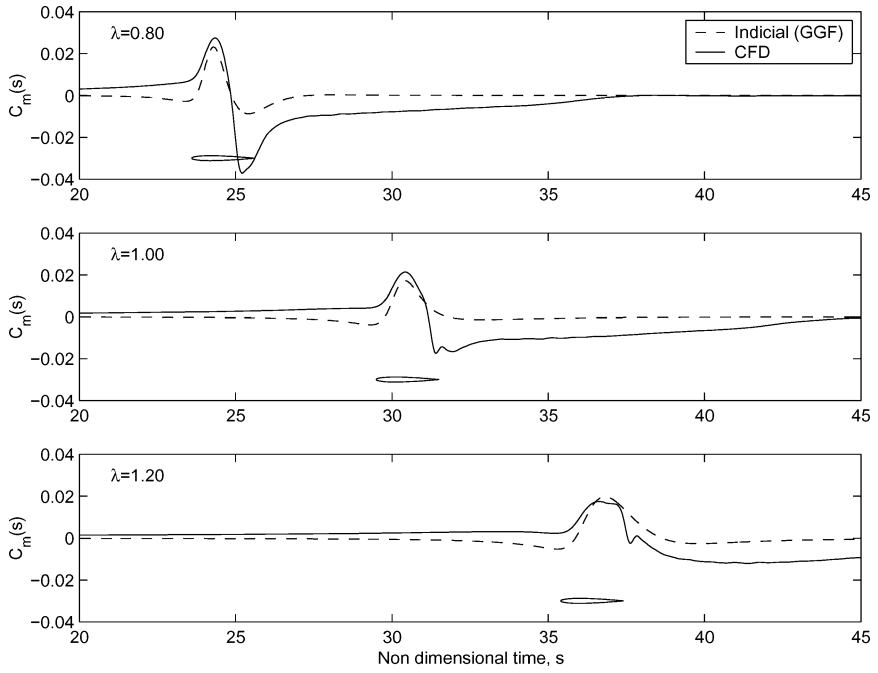

b) $M = 0.8$

Fig. 9 Moment response of AVI for $M = 0.5$ and 0.8 and $\lambda = 0.8$–1.2 ($Z_v = -0.25$ chords, $\bar{\Gamma} = 0.2$).

gives

$$\Psi_L(0, M, \lambda) = C_{l_\alpha}(1 + A_2 + A_3 + A_4) = 0 \tag{13}$$

Therefore, it follows that

$$A_4 = -1 - A_2 - A_3 \tag{14}$$

The exact value of the initial slope is found by differentiation of the exact value of lift response obtained by Singh.[10] This is evaluated as

$$\left.\frac{\mathrm{d}Cl}{\mathrm{d}s}\right|_{(s=0)} = \frac{2}{\sqrt{M\lambda^3}}\left[\frac{\lambda}{\lambda + (1-\lambda)M}\right]^{\frac{1}{2}} \tag{15}$$

Differentiation of the approximate function $\Psi_L(s, M, \lambda)$ chosen gives

$$\left.\frac{\mathrm{d}\Psi_L}{\mathrm{d}s}\right|_{(s=0)} = C_{l_\alpha}(A_1 - A_2 b_2 - A_3 b_3 - A_4 b_4) \tag{16}$$

From Eqs. (15) and (16), the value of b_4 can be found:

$$b_4 = \left(-\frac{\mathrm{d}Cl/\mathrm{d}s|_{(s=0)}}{Cl_\alpha} + A_1 - A_2 b_2 - A_3 b_3\right) \Big/ A_4 \tag{17}$$

The asymptotic quasi-steady value of $C_{l_\alpha} = 2\pi/\beta$ is automatically satisfied as $\Psi_L(M, \lambda, s) \to C_{l_\alpha}$ as $s \to \infty$. This is because all of the exponential terms of the function $\Psi_L(M, \lambda, s)$ go to zero as

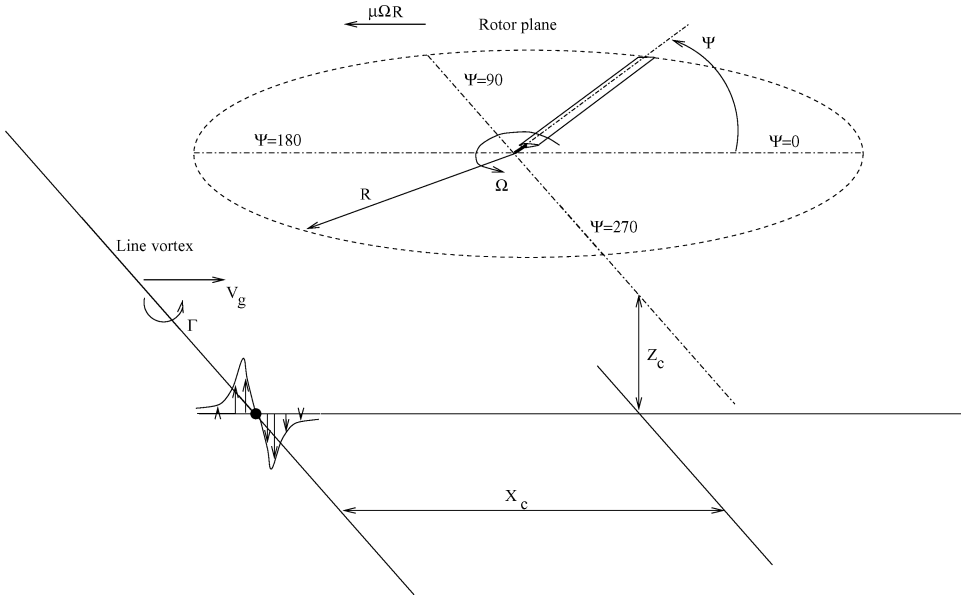

Fig. 10 BVI at 90 deg.

$s \to \infty$. For the optimization process, the lower limit of variation for the variables b_i were set to zero to prevent divergence. The constraints used for the pitching moment gust function $\Psi_M(M, \lambda, s)$ are analogous to those mentioned earlier.

Results and Discussion

Step Change in Angle of Attack and Pitch Rate for a Finite Wing

The lift and moment responses from the linearized model are compared to those from the corresponding CFD model for a range of Mach numbers. Representative solutions for a Mach number of 0.5 for a step change in angle of attack are presented to explain the trends. The indicial lift response from the linearized model is shown in Fig. 4a. Note that the sectionwise lift response initially closely follows the two-dimensional response at all sections. It is only later that the three-dimensional effect sets in, resulting in a spectrum. Results from direct Euler calculations with CFD for the same test case are shown in Fig. 4b. On the whole, there is good agreement, with CFD predicting slightly higher lift than that predicted from the linearized Weissinger-L model. Furthermore, because the Weissinger-L model assumes the flow is incompressible (so that induced velocities from the trailed wake are felt instantaneously) in the spanwise direction, it shows a faster buildup of the circulatory lift and, hence, attains steady state faster. Figure 5 shows the three-dimensional plot of the response to give a better picture of the flow physics. Note that both the CFD and Weissinger-L models attain the nearly elliptic distribution at the steady state, but that the Weissinger-L consistently underpredicts the lift for most spanwise locations. As was seen earlier, initially ($s = 0$) the lift remains constant, equal to the two-dimensional value at all sections, and later the tip loss effects set in. The sectionwise comparisons of the lift response for Mach numbers 0.5–0.8 are shown in Fig. 6a. Although there is good agreement at the lower Mach number case, there is an increasing disagreement between the solutions with increasing Mach number. Lift response from the CFD calculation does not converge to the linearized steady-state value of $2\pi/\beta$. Also, CFD calculations show a large nose-down pitching moment at the steady state. Such disparateness may be attributed to the nonlinear nature of the flowfield because of the transonic compressible effects and the movement of the aerodynamic center (assumed to be quarter-chord for linearized). From Fig. 6b it is clear that there is a spanwise variation of the aerodynamic center location. The aerodynamic center location at 43% chord, which was found from the two-dimensional CFD calculations, gives reasonable results for the root region. However, toward the tip, note that using an aerodynamic center location shifted to about 30% chord gives a better correlation with a CFD computed pitching moment. Pressure contours at two span stations, one toward the root and other toward the tip of the wing, are shown in Fig. 7. The pressure contours clearly indicate the presence of a strong shock toward the root of the wing. The strength of the shock progressively decreases toward the tip. This explains the shift of the aerodynamic center toward the leading edge moving toward the tip regions.

Airfoil–Vortex Interaction (AVI)

Studies of the unsteady lift and moment response of an airfoil interacting with a vortex is conducted to evaluate the accuracy of the generalized gust functions. Figure 2b shows the model problem. A point vortex is assumed to convect in a straight line at a fixed distance below an airfoil in freestream. The vortex strength is assumed to be of a constant prescribed value, and its structure is assumed to remain undistorted when interacting with the airfoil. Scully's[17] vortex-core model is used to avoid a singularity at the center of the vortex. The model is described as

$$V_\theta = \frac{\Gamma r}{2\pi\left(r_c^2 + r^2\right)} \tag{18}$$

where V_θ is the tangential velocity, r is the radial distance from the center, and r_c is the core radius, which is assumed to be 15% of the airfoil chord. Γ is the nondimensional vortex strength, nondimensionalized with airfoil chord and freestream velocity. The unsteady loads are calculated with a recursive algorithm[10,18,19] for the Duhamel integration of the indicial response functions. Direct inviscid Euler computations are also performed to verify the results obtained from the indicial model.

The unsteady effects of AVI can be thought of as effects caused by the airfoil penetrating through a series of gusts of nonequal magnitude at different instances of time. The highest amount of noncirculatory lift buildup occurs when the vortex is directly beneath the airfoil, and these effects progressively decay with time. The vortex is initialized 15 chords upstream at $s = 0$. From Fig. 8, note that the lift response from the indicial and CFD models show good agreement. They almost perfectly match until the vortex interacts with the blade. After that, there is a small disparity between the lift time history curves owing to the slight discrepancies between the CFD indicial response and the optimized approximate gust function response in the intermediate overlap region between the intial region and the steady-state region. The agreement also deteriorates with higher Mach number as flowfield nonlinearities develop and as the quality of the approximate gust function deteriorates. Another possible source of the disrepancy is the changing horizontal velocity field, which is included in the CFD calculations but is

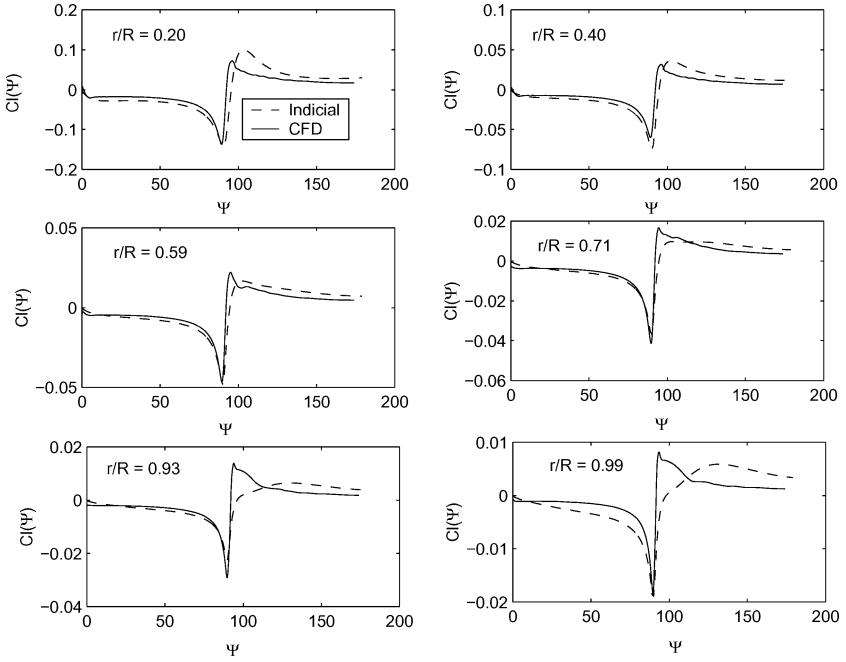

a) Lift response

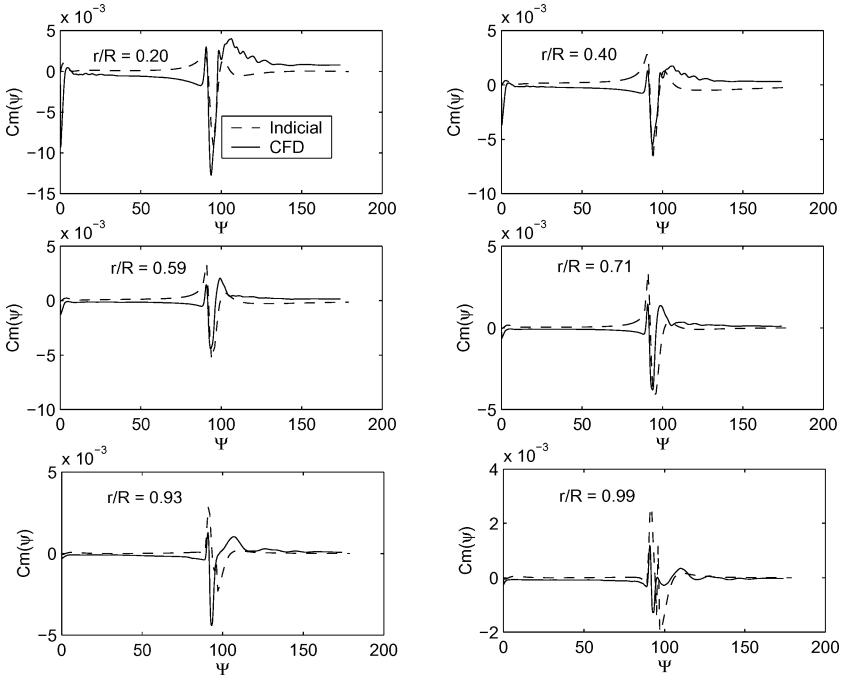

b) Pitching moment response

Fig. 11 Response to parallel BVI(M_{tip}, μ, λ_g) = (0.7, 0.2, 1.0).

neglected in the linearized aerodynamic calculations. Fortunately, the slope of the lift with respect to time, during the main part of the vortex interaction, remains well predicted by the linearized aerodynamics over the shown range of Mach number and gust ratio. This is important for calculation of the resulting acoustics because it is dominated by the time derivative of the lift. Figures 9 show the pitching moment response to AVI. Although the results from the CFD and indicial models show good agreement, the agreement is not as good as for the lift response case. The qualitative nature of the curves look similar, but there is considerable discrepancy in the peak magnitudes immediately after the interaction. This could be because the effects of nonlinearities are more pronounced in the moment response because the pitching moment is more sensitive to changes in the surface pressure distributions compared to the lift. Also, once again, the neglection of the change in pitching moment because of varying horizontal velocity in the linearized aerodynamic model may play a role in the discrepancy. Fortunately, the changes in moment response with respect to changes in the gust ratio are well captured. Traditionally, the moments caused by moving gusts are completely ignored in comprehensive rotor analysis codes.

Blade Vortex Interaction

Model Problem

Blade–vortex interaction (BVI) is the three-dimensional equivalent of AVI. The model problem chosen is shown in Fig. 10. A line vortex of infinite length is assumed to be convecting at a constant velocity V_g toward a rotor plane moving forward at $\mu\Omega R$, where R is the radius, μ is the advance ratio, and Ω is the angular velocity of the rotor blade. A miss distance Z_v of 0.25 chord was assumed for the study. The horizontal distance of the vortex from the rotor hub is so determined that a parallel BVI occurs at $\psi = 90$ deg. A

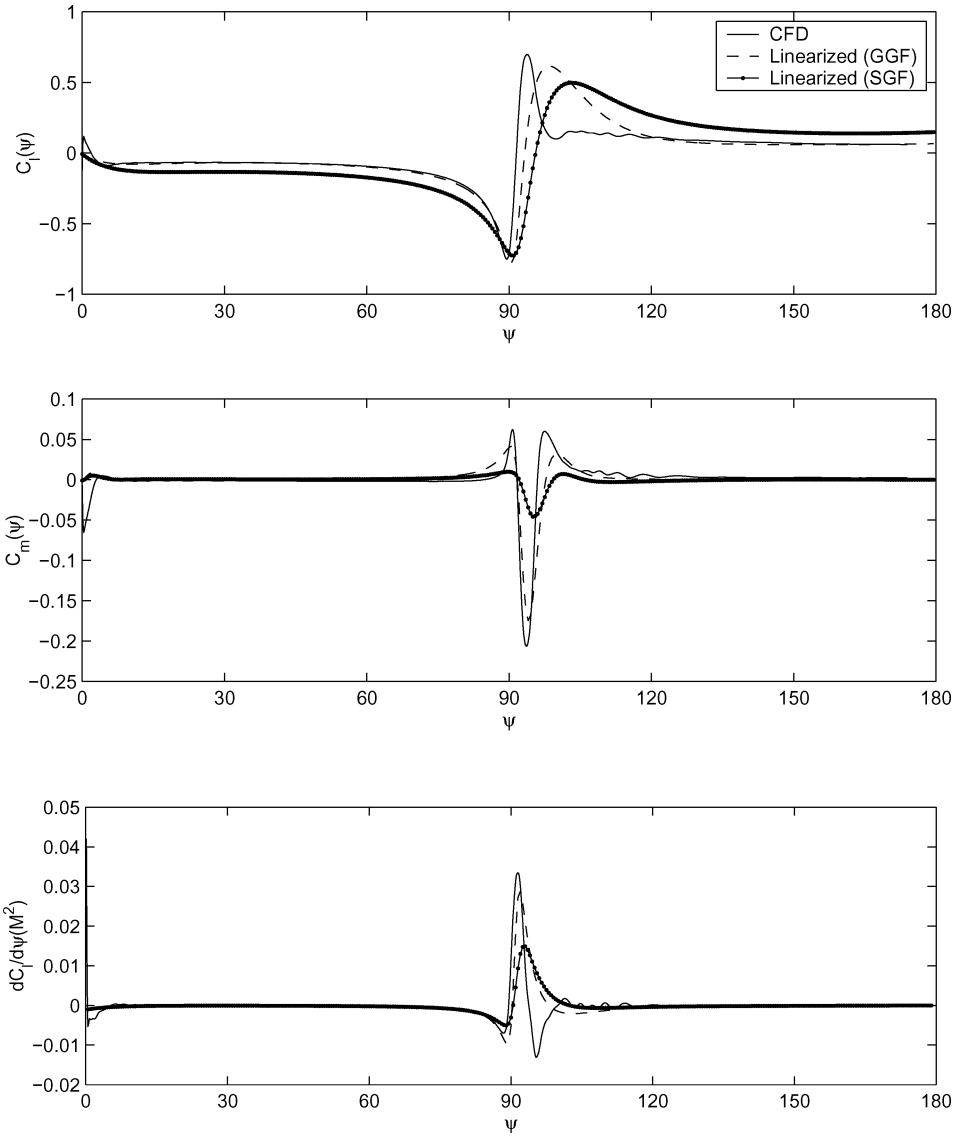

Fig. 12 Comparison of using SGF and GGF for BVI response prediction (M_{tip}, μ, λ_g) = (0.7, 0.2, 0.8) at span station $r/R = 0.40$.

parallel BVI, such as that described, is found to occur when a rotor blade interacts with the wake shed by its counterparts. The noise generated by such interactions, BVI noise, is a major contributor of rotorcraft noise during landing. To simplify the calculation, the blade is assumed to be nonlifting, except for the lift generated by the BVI.

Methodology

Investigation of the model problem chosen is conducted with both direct Euler calculations and the linearized Weissinger-L model. A rotor model similar to that used for the finite wing as show in Fig. 1 is used with the near-wake trailers extending along the azimuth. At each spanwise section, the Mach number M and the speed ratio λ are different. M and λ at a specific section at $x = r/R$ and at $\psi = 90$ are given by

$$M_{\text{tip}} = \frac{\Omega R}{a} \tag{19}$$

$$\lambda_g = \frac{\mu \Omega R}{V_g + \mu \Omega R} \tag{20}$$

$$M(x) = M_{\text{tip}}(x + \mu) \tag{21}$$

$$\lambda(x) = \frac{M(x)}{M(x) + V_g/a} \tag{22}$$

Because the unsteady response to this BVI problem is dominated by variations at $\psi = 90$ deg, it is justifiable to assume that the Mach number and speed ratio are nonvariant with azimuth ψ. With the generalized representation of the approximate gust function, the indicial coefficients at each section are determined. These are used for the computation of the unsteady load response at each section. Once the unsteady sectionwise loads are determined, the three-dimensional effects are coupled by the use of the Weissinger-L model, as described earlier.

Results

The sectionwise lift response for parallel BVI at 90 deg is shown in Fig. 11a. It can be seen that there is a large variation in the unsteady load peaks along the span. The lift response maintains the same shape as in the case of AVI. However, the unsteady fluctuations progressively decrease toward the tip. The lift response from the indicial method shows excellent agreement with CFD calculations at inboard locations of the blade. The disparity between the solutions increases progressively outboard. The Weissinger-L model, being based on a linearized incompressible vortex method, will not be able to account for the nonlinear tip effects exactly. This should be the reason for the higher disparity at the tips. The sectionwise moment response (Fig. 11b) shows behavior similar to that of the lift response, although the disparities in the solutions are higher because the pitching moments are more sensitive to nonlinearities

in surface pressure distributions. A comparison of stationary gust functions (SGF) (where speed ratio is assumed to be one regardless of radial location) and GGF in predicting the BVI response is shown for $M_{\text{tip}} = 0.7$, $\mu = 0.2$, and $\lambda_g = 0.8$ in Fig. 12. Note that the GGF predicts the responses better than the SGF. Although there is not much difference in the lift response case, the SGF considerably underpredicts the pitching moment peaks because the pitching moment is more sensitive to a faster moving gust. Also, the comparison of lift-time derivatives indicate that the faster moving gust causes greater variations in the derivatives, which is captured well by the GGF compared to the SGF. On the whole, it is clear that the indicial methods that use GGF are sufficient to predict the airloads during a parallel BVI, at least for the configuration studied here.

Conclusions

The fidelity of linearized indicial methods for aerodynamic load prediction is investigated. It is found that the linearized methods are sufficiently accurate to be used as a practical design tool, even in transonic flow regimes. Although direct Euler calculations are more accurate in predicting the aerodynamic responses caused by unsteady forcing, they require enormously large computational resources and time to be used in practical applications. The GGF developed for pitching moment and lift in terms of speed ratio and freestream Mach number should facilitate the use of linearized load prediction schemes for more complicated problems, such as a rotor blade interacting with a complex wake structure. Future studies will be concentrated on the interaction of rotor blades with a more realistic wake structure, as well as on the aerodynamics of oblique interactions, to better understand and enhance the accuracy of indicial methods.

Acknowledgments

This work was supported by the U.S. Army Research Office.

References

[1]Leishman, J. G., "Subsonic Unsteady Aerodynamics Caused by Gusts Using the Indicial Method," *Journal of Aircraft*, Vol. 33, No. 5, 1996, pp. 869–879.

[2]Bisplinghoff, R. L., Ashley, H., and Halfman, R. L., *Aeroelasticity*, Addison–Wesley, Reading, MA, 1995, Chap. 6, pp. 294–375.

[3]Lomax, H., Heaslet, M. A., Fuller, F. B., and Sluder, L., "Two and Three Dimensional Unsteady Lift Problems in High Speed Flight," NACA Rept. 1077, Jan. 1952.

[4]Lomax, H., "Indicial Aerodynamics," *AGARD Manual of Aeroelasticity*, Pt. 2, 1968, Chap. 6.

[5]Mazelsky, B., "Determination of Indicial Lift and Moment of a Two-Dimensional Pitching Airfoil at Subsonic Mach Numbers from Oscillatory Coefficients with Numerical Calculations for a Mach number of 0.7," NACA TN 2613, Feb. 1952.

[6]Miles, J. W., "The Aerodynamic Force on an Airfoil in a Moving Gust," *Journal of Aeronautical Sciences*, Vol. 23, No. 11, 1956, pp. 1044–1050.

[7]Drischler, J. A., and Diederich, F. W., "Lift and Moment Responses to Penetration of Sharp-Edged Traveling Vertical Gusts, with Application to Penetration of Weak Blast Waves," NACA TN 3956, May 1957.

[8]Mazelsky, B., and Drischler, J. A., "Numerical Determination of Indicial Lift and Moment Functions for a Two-Dimensional Sinking and Pitching Airfoil at Mach Numbers 0.5 and 0.6," NASA TN 2739, July 1952.

[9]Leishman, J. G., "Unsteady Aerodynamics of Airfoils Encountering Traveling Gusts and Vortices," *Journal of Aircraft*, Vol. 34, No. 6, 1997, pp. 719–729.

[10]Singh, R., "Transonic Effects on Aerodynamics and Acoustics of Blade–Vortex Interaction," Ph.D. Dissertation, Dept. of Aerospace Engineering, Univ. of Maryland, College Park, MD, Dec. 1999.

[11]Evvard, J. C., "Use of Source Distribution for Evaluating Theoretical Aerodynamics of Thin Finite Wings at Supersonic Speeds," NACA Rept. 951, June 1950.

[12]Singh, R., and Baeder, J. D., "The Direct Calculation of Indicial Lift Response of a Wing Using Computational Fluid Dynamics," *Journal of Aircraft*, Vol. 35, No. 4, 1997, pp. 465–471.

[13]Singh, R., and Baeder, J. D., "Generalized Moving Gust Response Using CFD with Application to Airfoil-Vortex Interaction," *Proceedings of the 15th AIAA Applied Aerodynamics Conference*, Atlanta, GA, June 1999; also AIAA Paper 97-2208.

[14]Srinivasan, G. R., and Baeder, J. D., "TURNS: A Free Wake Euler/Navier–Stokes Numerical Method for Helicopter Rotors," *AIAA Journal*, Vol. 31, No. 5, 1993, pp. 959–962.

[15]Baeder, J. D., and Srinivasan, G. R., "Computational Aeroacoustics Study of Isolated Blade–Vortex Interaction Noise," American Helicopter Society Aeromechanics Specialists Conf., Jan. 1994.

[16]Bagai, A., "Contribution of Mathematical Modeling of Rotor-Flow-Fields Using Pseudo-Implicit Free Wake Analysis," Ph.D. Dissertation, Dept. of Aerospace Engineering, Univ. of Maryland, College Park, MD, Aug. 1995.

[17]Scully, M. P., "Computation of Helicopter Rotor Wake Geometry and Its Influence on Rotor Harmonic Airloads," ASRL TR 178-1, Dept. of Aerospace Engineering, Massachusetts Inst. of Technology, Cambridge, MA, March 1975.

[18]Beddoes, T. S., "Practical Computation of Unsteady Lift," *Vertica*, Vol. 8, No. 1, 1984, pp. 55–71.

[19]"DOT Users Manual," ver. 4.00, Vanderplaats, Miura and Associates, Inc., April 1993.

[20]Leishman, J. G., "Validation of Approximate Indicial Aerodynamics Functions for Two-Dimensional Subsonic Flow," *AIAA Journal*, Vol. 25, No. 10, 1988, pp. 914–922.